Rotational structures in ^{129}Nd and signature splitting systematics of the $\nu h_{11/2}$ bands in $A \sim 130$ nuclei

O. Zeidan, D. J. Hartley, L. L. Riedinger, M. Danchev,* W. Reviol,† W. D. Weintraub,‡ and Jing-ye Zhang
Department of Physics and Astronomy, University of Tennessee, Knoxville, Tennessee 37996

A. Galindo-Uribarri, C. J. Gross, S. D. Paul,§ C. Baktash, M. Lipoglavsek,‖ D. C. Radford, and C. H. Yu
Physics Division, Oak Ridge National Laboratory, Oak Ridge, Tennessee 37831

D. G. Sarantites and M. Devlin¶
Chemistry Department, Washington University, St. Louis, Missouri 63130

M. P. Carpenter, R. V. F. Janssens, and D. Seweryniak
Physics Division, Argonne National Laboratory, Argonne, Illinois 60439

E. Padilla
Instituto de Ciencias Nucleares, UNAM, 04510 Mexico, D.F., Mexico

High-spin states in ^{129}Nd were populated in the reaction ^{92}Mo(^{40}Ca,$2pn$) with beam energies of 170 and 184 MeV in two separate experiments. Over 140 new transitions were placed in a level scheme that consists of four rotational structures, three of which have been observed for the first time. The bands were assigned configurations based on their $B(M1)/B(E2)$ ratios (for the strongly coupled bands), aligned angular momentum, observed band crossings, and signature splitting. Evidence for of the observation of the deformation driving $\nu i_{13/2}[660]1/2$ orbital is presented. Signature splitting trends in the $\nu h_{11/2}$ bands of $A \sim 130$ nuclei are investigated within the framework of the cranked shell model. Comparisons are made with observations in the $\pi h_{11/2}$ bands near $A \sim 160$.

I. INTRODUCTION

The mass 130 region, with $Z \sim 60$ and $N \sim 74$, is well known for shape competition between weakly prolate and oblate bands at low spin [1], and for the occurrence of highly deformed bands at higher spins [2–7]. This is due to the soft core, which is susceptible to shape driving forces of the valence nucleons. The occupation of the $\nu i_{13/2}$ orbitals or of a hole in the $\pi g_{9/2}$ orbitals enhances the deformation of these nuclei from $\beta_2 \sim 0.2$ to $\beta_2 \sim 0.3$–0.4 [8,9]. The alignment of two high-K $h_{11/2}$ neutrons was associated with driving the nucleus to oblate shapes [10], while the occupation of one neutron in a $\nu h_{11/2}$ orbital, outside the even-even core, may produce a stable triaxial deformation [11].

Although the $N \sim 74$ nuclei were well studied through the use of Xn reaction channels, the lighter nuclei with $N \leq 70$

are not as well known. This is mainly due to lower cross-section reactions, and to the fact that the neutron-deficient compound nuclei favor multiple charged-particle reaction channels, which can produce over 20 different species of nuclei. However, with the sensitivity of Gammasphere [12] and the selectivity of the Microball [13], it is now possible to explore these nuclei which are far from stability.

In an experiment designed to populate high-spin states in the mass 130 region, a ^{92}Mo target was bombarded with ^{40}Ca. Theoretical calculations [14] predicted large ground-state deformations $\beta_2 \sim 0.3$ for $Z \sim 60$, $N \leq 70$ nuclei, which is nearly as large as the highly deformed bands found in the heavier $A \sim 130$ region. Therefore, it is of interest to look for bands with the same highly deformed configuration (namely, $\nu i_{13/2}$ structure) in lighter nuclei to compare with those observed near $N \sim 74$. The large ground-state deformation essentially eliminates the possibility of seeing oblate bands at low spin; however, one can track the shape driving influence of the $h_{11/2}$ neutron as N is decreased and β_2 is increased.

This paper will focus on the nucleus $^{129}_{60}$Nd$_{69}$, which is the lightest odd-A neodymium nucleus known. A significant extension of the level scheme was achieved by adding over 140 new transitions and three new structures to the previous work [15]. Evidence of the intruder $i_{13/2}$ band is indeed observed in ^{129}Nd as it adiabatically crosses a normal deformed sequence. A signature splitting in the energy levels of the $\nu h_{11/2}$ band was observed and compared with other $\nu h_{11/2}$ bands in the region. As signature splitting in these high-K

*Permanent address: Faculty of Physics, St. Kliment Ohridsky University of Sofia, BG-1164, Sofia, Bulgaria.

†Present address: Chemistry Department, Washington University, St. Louis, MO 63130.

‡Present address: Department of Physics, Florida State University, Tallahassee, FL 32306.

§Present address: Department of Nuclear and Atomic Physics, Tata Institute of Fundamental Research, Mumbai 400 005, India.

‖Present address: J. Stefan Institute, Ljubljana, Slovenia.

¶Present address: Los Alamos National Laboratory, Los Alamos, NM 87545.

bands is thought to be a result of significant γ deformation, cranked shell-model calculations were performed in order to reveal approximate magnitudes and trends of triaxiality as a function of proton and neutron number.

II. EXPERIMENTAL DETAILS

Ions of ^{129}Nd were produced using the reaction ^{92}Mo(^{40}Ca,2pn). In one experiment, the 170-MeV ^{40}Ca beam was supplied by the 25-MV tandem accelerator at the Holifield Radioactive Ion Beam Facility (HRIBF) at Oak Ridge National Laboratory (ORNL). The self-supporting ^{92}Mo target had a thickness of $\sim 450 \mu$g/cm^2. The emitted gamma rays were detected by the Ge Clover detector array CLARION [16], consisting of 11 segmented clover spectrometers within bismuth germanate anti-Compton shields, and ten single-volume detectors. Protons and α particles emitted by the deexciting compound nuclei were identified using a HyBall [16] array consisting of 95 CsI scintillators (coupled to photodiodes) in a 4π geometry. Reaction products recoiling from the target foil were separated by the recoil mass spectrometer (RMS) [17–19] at the focal plane according to their mass-to-charge ratio. The RMS has acceptances of $\pm 10\%$ in the recoil ion energy and $\pm 5\%$ in the mass-to-charge ratio A/Q. A multiwire, gas-filled position sensitive avalanche counter (PSAC) [16,17] was used to observe the spatial distribution of the mass groups at the focal plane. The RMS was tuned for central recoils of mass $A = 129$, with an energy of 40.5 MeV and a charge state $Q = 20.5^+$. The data were taken using a γ-γ-recoil trigger that required at least two HPGe detectors in prompt coincidence with a recoil signal from the PSAC. Gamma rays associated

with mass 129 were sorted into a symmetric $E_\gamma \times E_\gamma$ coincidence matrix, and were subsequently analyzed with the RADWARE software package [20]. A matrix of E_γ versus charged-particle multiplicity, with the same mass-gated condition, was also sorted such that gamma-charged particle coincidences could be investigated. A total of ~ 4.2 million γ-γ coincidences were observed in the $A = 129$ mass-gated matrix.

In a second experiment, emphasizing the population of the highest spin states possible, a 184 MeV ^{40}Ca beam from the ATLAS superconducting linear accelerator at Argonne National Laboratory (ANL) was delivered to a 0.625-mg/cm^2-thick, self-supporting ^{92}Mo target. Prompt γ rays were detected with 99 Compton-suppressed Ge spectrometers in the Gammasphere array. Charged-particle evaporation residues were detected with the 95 CsI detectors of the Washington University Microball array [13]. Approximately 116 million fivefold (γ^5) or higher events were determined to have gamma rays in coincidence with only two protons (comprising $\sim 20\%$ of the total events). These events were sorted into an $E_\gamma \times E_\gamma \times E_\gamma$ coincidence cube, and were analyzed with the Radware software package. The level scheme for ^{129}Nd from the present data is shown in Fig. 1.

Relative spin assignments proposed for the states in ^{129}Nd were determined through directional correlation of oriented states (DCO) analysis. An asymmetric matrix was sorted from the Gammasphere data, where the energy of γ rays observed in detectors located at $\sim 35°$ and $\sim 145°$ were histogrammed along one axis, and coincident γ rays observed in detectors located at $\sim 90°$ were histogrammed along the other. DCO ratios were determined by the expression

$$R_{DCO} = \frac{I_{\gamma_1}(\text{at} \sim 35° \text{ or} \sim 145°; \text{ in coincidence with } \gamma_2 \text{ at } 90°)}{I_{\gamma_1}(\text{at } 90°; \text{ in coincidence with } \gamma_2 \text{ at} \sim 35° \text{ or} \sim 145°)},$$

where I_{γ_1} is the intensity of the γ ray of interest and γ_2 is a stretched $E2$ ($\Delta I = 2$) transition. With the detectors at the given angles, one expects R_{DCO} values of approximately 0.5 for pure dipole transitions ($M1$ and $E1$) and 1.0 for quadrupole transitions ($E2$). The measured DCO ratios are summarized in Table I along with the energy, spin, branching ratio, and parity of the states, as well as the energy and relative intensity of the depopulating γ rays. Weak transitions above states of determined spin, where reliable DCO analysis could not be performed, were assigned multipolarities assuming that the rotational behavior of the band persists, and the spins are shown in parentheses in Fig. 1.

A spectrum of $A = 129$ transitions from the ORNL data is presented in Fig. 2. Transitions in coincidence with both $A = 129$ recoils and three protons (^{129}Pr) have been subtracted from the spectrum, leaving possible transitions from ^{129}Nd ($2pn$), ^{129}Pm ($p2n$), and ^{129}Sm ($3n$). However, no evi-

dence of the latter two nuclei was observed, and all the transitions in Fig. 2 were accounted for in the level scheme of ^{129}Nd (see Fig. 1). Relative cross sections (with respect to the strongest channel ^{129}Pr) were determined in the ORNL experiment and compared with theoretical predictions from HIVAP [21]. Good agreement was found for most of the channels, and therefore, the calculated cross section of ~ 50 mb is likely a reasonable estimate for the $2pn$ channel leading to ^{129}Nd.

III. LEVEL SCHEME

Before the present work, little was known about ^{129}Nd. Watson *et al.* [15] reported observing a strongly coupled sequence, and assigned it to ^{129}Nd. In addition to confirming and extending the previously known sequence to higher
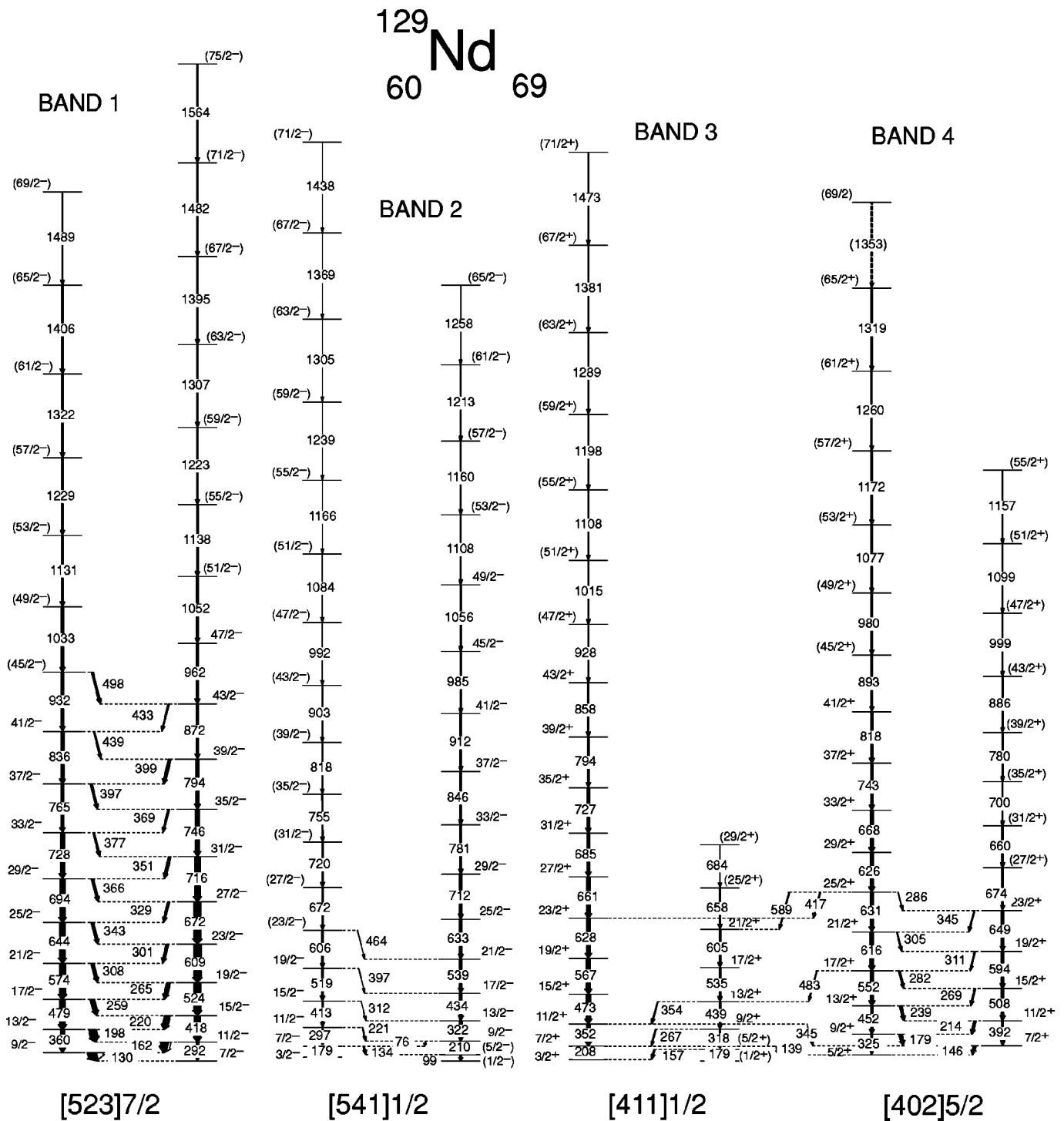
FIG. 1. The level scheme for ^{129}Nd. The width of the arrows is proportional to the relative intensity of the transitions. Tentative transitions are denoted by dashed lines. Spin and parity assignments are explained in the text. The proposed band-head configurations are also given.

spins (labeled band 1 in Fig. 1), over 140 new transitions and three new structures were observed.

One may see in Fig. 1 that the positive-parity structures, bands 3 and 4, are linked with each other, while the negative-parity structures, bands 1 and 2, are not connected to any of the observed sequences. Previous decay works [22,23] suggested a ground-state spin of $(\frac{5}{2}^{+})$ as well as a $(\frac{7}{2}^{-})$ or $(\frac{9}{2}^{-})$

isomeric state. From our analysis of the high-spin states, it is not clear whether any of the observed structures feeds the ground state and therefore, firm excitation energies, spins, and parities cannot be assigned. However, the four structures have in-band characteristics that are similar to the four strongest bands in ^{131}Nd [24]. Thus spin and parity assignments are largely based on systematics and similarities with ^{131}Nd

TABLE I. Data for levels and γ rays in ^{129}Nd.

$I_i^{\pi\,a}$	E_{level} (keV)[b]	E_γ (keV)[c]	I_γ[d]	DCO	λ[e]	Multipolarity
Band 1 : [523]7/2 $\alpha=+\frac{1}{2}$						
$\frac{9}{2}^-$	$X+130.5$	130.5	N/D[f]	0.63(4)		$M1/E2$
$\frac{13}{2}^-$	$X+491.0$	360.5	53(3)	1.0(1)	0.51(3)	$E2$
		198.6	96(5)	0.56(3)		$M1/E2$
$\frac{17}{2}^-$	$X+969.6$	478.6	78(4)	0.91(8)	1.17(7)	$E2$
		259.0	58(3)	0.47(5)		$M1/E2$
$\frac{21}{2}^-$	$X+1542.8$	573.2	76(4)	0.96(7)	1.8(1)	$E2$
		308.1	42(2)	0.45(2)		$M1/E2$
$\frac{25}{2}^-$	$X+2187.0$	644.2	75(4)	1.14(8)	2.1(1)	$E2$
		343.4	29(2)	0.57(3)		$M1/E2$
$\frac{29}{2}^-$	$X+2881.4$	694.4	71(4)	0.99(4)	3.7(4)	$E2$
		365.6	23(1)			$M1/E2$
$\frac{33}{2}^-$	$X+3609.5$	728.1	59(4)	1.04(4)	2.5(2)	$E2$
		377.1	22(1)			$M1/E2$
$\frac{37}{2}^-$	$X+4374.1$	764.6	38(2)	1.1(1)	3.3(4)	$E2$
		396.0	13.7(6)			$M1/E2$
$\frac{41}{2}^-$	$X+5210.3$	836.2	33(2)	0.9(1)	5.3(8)	$E2$
		438.3	8.8(9)			$M1/E2$
$(\frac{45}{2}^-)$	$X+6142.4$	932.1	22(2)		2.6(3)	$E2$
		498.5	6(1)			$M1/E2$
$(\frac{49}{2}^-)$	$X+7175.5$	1033.1	18(2)			$E2$
$(\frac{53}{2}^-)$	$X+8306.8$	1131.3	12(1)			$E2$
$(\frac{57}{2}^-)$	$X+9535.1$	1228.3	8(1)			$E2$
$(\frac{61}{2}^-)$	$X+10857.1$	1322.0	6(1)			$E2$
$(\frac{65}{2}^-)$	$X+12263.0$	1405.9	5(1)			$E2$
$(\frac{69}{2}^-)$	$X+13746$	1483	<4			$E2$
Band 1 : [523]7/2 $\alpha=-\frac{1}{2}$						
$\frac{7}{2}^-$	X					
$\frac{11}{2}^-$	$X+292.5$	292.5	30(2)	0.72(6)	0.40(2)	$E2$
		162.5	124(7)	0.51(3)		$M1/E2$
$\frac{15}{2}^-$	$X+710.6$	418.1	75(4)	0.94(7)	1.12(6)	$E2$
		219.8	77(4)	0.47(4)		$M1/E2$
$\frac{19}{2}^-$	$X+1234.9$	524.3	$\equiv100$	0.99(9)	1.88(7)	$E2$
		265.6	47(2)	0.40(7)		$M1/E2$
$\frac{23}{2}^-$	$X+1843.7$	608.8	91(5)	0.98(5)	4.0(2)	$E2$
		300.9	32(2)	0.43(5)		$M1/E2$
$\frac{27}{2}^-$	$X+2516.0$	672.3	84(5)	1.04(7)	3.0(2)	$E2$
		329.0	24(1)			$M1/E2$
$\frac{31}{2}^-$	$X+3232.2$	716.2	72(4)	0.94(4)	3.5(3)	$E2$
		351.0	24(2)			$M1/E2$
$\frac{35}{2}^-$	$X+3978.5$	746.3	51(3)	0.92(6)	4.4(5)	$E2$
		368.6	21(1)			$M1/E2$
$\frac{39}{2}^-$	$X+4772.0$	793.5	38(2)	0.91(7)	2.1(3)	$E2$
		398.0	13(1)			$M1/E2$
$\frac{43}{2}^-$	$X+5644.5$	872.5	24(2)	0.92(3)		$E2$
		433.0	6.7(7)			$M1/E2$
$\frac{47}{2}^-$	$X+6606.6$	962.1	19(2)	0.91(6)		$E2$
$(\frac{51}{2}^-)$	$X+7658.5$	1051.9	13(1)			$E2$
$(\frac{55}{2}^-)$	$X+8796.9$	1138.4	12(1)			$E2$

TABLE I. (*Continued*).

I_i^{π} [a]	E_{level} (keV) [b]	E_{γ} (keV) [c]	I_{γ} [d]	DCO	λ [e]	Multipolarity
$(\frac{59}{2}^-)$	$X+10019.6$	1222.7	9(1)			$E2$
$(\frac{63}{2}^-)$	$X+11326.6$	1307.0	7(1)			$E2$
$(\frac{67}{2}^-)$	$X+12720.6$	1394.0	5(1)			$E2$
$(\frac{71}{2}^-)$	$X+14202$	1482	<4			$E2$
$(\frac{75}{2}^-)$	$X+15765$	1563	<4			$E2$

Band 2 : [541]1/2 $\alpha=+\frac{1}{2}$

I_i^{π} [a]	E_{level} (keV) [b]	E_{γ} (keV) [c]	I_{γ} [d]	DCO	λ [e]	Multipolarity
$\frac{1}{2}^-$	Y					
$\frac{5}{2}^-$	$Y+99.0$	99.0	18(9)	1.0(1)		$E2$
$\frac{9}{2}^-$	$Y+308.5$	209.5	37(7)	0.96(7)	13.0(1)	$E2$
		76.0	4(1)			$M1/E2$
$\frac{13}{2}^-$	$Y+630.9$	322.4	38(3)	0.87(7)		$E2$
$\frac{17}{2}^-$	$Y+1064.9$	434.0	30(2)	1.01(7)		$E2$
$\frac{21}{2}^-$	$Y+1604.0$	539.1	28(2)	1.12(4)		$E2$
$\frac{25}{2}^-$	$Y+2237.1$	633.1	26(2)	0.93(7)		$E2$
$\frac{29}{2}^-$	$Y+2949.4$	712.3	25(2)	0.94(7)		$E2$
$\frac{33}{2}^-$	$Y+3730.6$	781.2	17(1)	1.09(7)		$E2$
$\frac{37}{2}^-$	$Y+4575.9$	845.3	12(1)	1.05(6)		$E2$
$\frac{41}{2}^-$	$Y+5487.7$	911.8	9(1)	1.06(5)		$E2$
$\frac{45}{2}^-$	$Y+6472.3$	984.6	8(1)	0.99(8)		$E2$
$\frac{49}{2}^-$	$Y+7528.3$	1056.0	6(1)	1.1(1)		$E2$
$(\frac{53}{2}^-)$	$Y+8637$	1108	<4			$E2$
$(\frac{57}{2}^-)$	$Y+9797$	1160	<4			$E2$
$(\frac{61}{2}^-)$	$Y+11010$	1213	<4			$E2$
$(\frac{65}{2}^-)$	$Y+12266$	1256	<4			$E2$

Band 2 : [541]1/2 $\alpha=-\frac{1}{2}$

I_i^{π} [a]	E_{level} (keV) [b]	E_{γ} (keV) [c]	I_{γ} [d]	DCO	λ [e]	Multipolarity
$\frac{3}{2}^-$	$Y+54$					
$\frac{7}{2}^-$	$Y+178.8$	178.8	12(2)	1.0(2)	2.92(4)	$E2$
		133.6	14(9)	0.9(2)		$M1/E2$
$\frac{11}{2}^-$	$Y+476.3$	297.5	18(2)	1.1(1)	4.5(3)	$E2$
		221.50	9(1)			$M1/E2$
$\frac{15}{2}^-$	$Y+888.9$	412.6	20(2)	1.0(1)	19(3)	$E2$
		312.0	<4			$M1/E2$
$\frac{19}{2}^-$	$Y+1407.7$	518.8	25(2)	1.0(3)	10(1)	$E2$
		397.2	5(1)			$M1/E2$
$(\frac{23}{2}^-)$	$Y+2013.5$	605.8	22(2)		12(1)	$E2$
		464.0	<4			$M1/E2$
$(\frac{27}{2}^-)$	$Y+2685.2$	671.7	21(3)			$E2$
$(\frac{31}{2}^-)$	$Y+3405.2$	720.0	19(2)			$E2$
$(\frac{35}{2}^-)$	$Y+4160.3$	755.1	16(1)			$E2$
$(\frac{39}{2}^-)$	$Y+4978.3$	818.0	10(1)			$E2$
$(\frac{43}{2}^-)$	$Y+5881.2$	902.9	9(1)			$E2$
$(\frac{47}{2}^-)$	$Y+6873.1$	991.9	8(1)			$E2$
$(\frac{51}{2}^-)$	$Y+7956.8$	1083.7	7(1)			$E2$
$(\frac{55}{2}^-)$	$Y+9122.8$	1166.0	5(1)			$E2$
$(\frac{59}{2}^-)$	$Y+10361.9$	1239.1	4(1)			$E2$

TABLE I. (*Continued*).

$I_i^{\pi\,a}$	E_{level} (keV)[b]	E_γ (keV)[c]	$I_\gamma{}^d$	DCO	λ^e	Multipolarity
$(\frac{63}{2}^-)$	$Y+11667$	1305	<4			$E2$
$(\frac{67}{2}^-)$	$Y+13036$	1369	<4			$E2$
$(\frac{71}{2}^-)$	$Y+14474$	1438	<4			$E2$

BAND 3 : [411]1/2 $\alpha=+\frac{1}{2}$

$\frac{1}{2}^+$	Z					
$\frac{5}{2}^+$	$Z+178.8$	178.8	6(1)		0.51(4)	$E2$
		157.0	14(2)	0.55(5)		$M1/E2$
$\frac{9}{2}^+$	$Z+497.2$	318.4	13.7(9)	1.02(9)	1.23(9)	$E2$
		267.5	8(1)	0.9(1)		$M1/E2$
$\frac{13}{2}^+$	$Z+936.3$	439.1	25(2)	0.91(7)	3.53(3)	$E2$
		354.3	9(1)			$M1/E2$
$\frac{17}{2}^+$	$Z+1471.7$	535.4	25(2)	0.9(1)		$E2$
$\frac{21}{2}^+$	$Z+2076.4$	604.7	23(2)	1.1(2)		$E2$
$(\frac{25}{2}^+)$	$Z+2734.7$	658.3	16(2)			$E2$
$(\frac{29}{2}^+)$	$Z+3418.4$	683.7	<4			$E2$

Band 3 : [411]1/2 $\alpha=-\frac{1}{2}$

$\frac{3}{2}^+$	$Z+22$					
$\frac{7}{2}^+$	$Z+208.2$	208.2	53(9)	0.95(5)	5.92(7)	$E2$
		138.8	13(4)	0.43(6)		$M1/E2$
$\frac{11}{2}^+$	$Z+559.8$	351.6	75(4)	0.94(5)	7.09(7)	$E2$
		344.8	5.7(6)	0.71(9)		$E2$
$\frac{15}{2}^+$	$Z+1032.5$	472.7	65(4)	1.09(7)		$E2$
$\frac{19}{2}^+$	$Z+1599.1$	566.6	57(3)	0.97(6)		$E2$
$\frac{23}{2}^+$	$Z+2227.1$	628.0	54(3)	0.95(6)		$E2$
$\frac{27}{2}^+$	$Z+2888.4$	661.3	48(3)	1.10(5)		$E2$
$\frac{31}{2}^+$	$Z+3573.1$	684.7	33(2)	0.93(5)		$E2$
$\frac{35}{2}^+$	$Z+4299.9$	726.8	32(2)	1.05(5)		$E2$
$\frac{39}{2}^+$	$Z+5094.5$	794.6	21(1)	1.10(6)		$E2$
$\frac{43}{2}^+$	$Z+5952.3$	857.8	15(1)	1.05(6)		$E2$
$(\frac{47}{2}^+)$	$Z+6879.9$	927.6	9.9(4)			$E2$
$(\frac{51}{2}^+)$	$Z+7895.1$	1015.2	8.7(9)			$E2$
$(\frac{55}{2}^+)$	$Z+9002.7$	1107.6	7.1(8)			$E2$
$(\frac{59}{2}^+)$	$Z+10200.9$	1198.2	4.9(7)			$E2$
$(\frac{63}{2}^+)$	$Z+11489.8$	1288.9	4.5(2)			$E2$
$(\frac{67}{2}^+)$	$Z+12871$	13801	<4			$E2$
$(\frac{71}{2}^+)$	$Z+14344$	1473	<4			$E2$

Band 4 : [402]5/2 $\alpha=+\frac{1}{2}$

$\frac{5}{2}^+$	$Z+91$					
$\frac{9}{2}^+$	$Z+415.5$	324.5	28(2)	0.97(6)	0.84(7)	$E2$
		179.1	32(3)	0.43(7)		$M1/E2$
$\frac{13}{2}^+$	$Z+868.2$	452.7	32(2)	0.88(6)	1.3(1)	$E2$
		239.3	22(2)	0.72(5)		$M1/E2$
$\frac{17}{2}^+$	$Z+1419.5$	551.3	36(3)	1.00(8)	2.5(1)	$E2$
		282.1	17(1)	0.72(9)		$M1/E2$
		482.6	<4	0.9(1)		$E2$

TABLE I. (*Continued*).

I_i^{π} [a]	E_{level} (keV) [b]	E_γ (keV) [c]	I_γ [d]	DCO	λ [e]	Multipolarity
$\frac{21}{2}^+$	$Z+2034.6$	615.1	34(3)	1.15(9)	2.9(2)	$E2$
		304.7	9.9(8)	0.69(9)		$M1/E2$
$\frac{25}{2}^+$	$Z+2665.7$	631.1	38(3)	1.01(6)	8.0(9)	$E2$
		286.9	5.5(7)	0.5(1)		$M1/E2$
		417.8	5.0(9)	0.63(7)		$M1/E2$
		589.2	9(1)	0.9(1)		$E2$
$\frac{29}{2}^+$	$Z+3292.3$	626.6	36(3)	0.88(5)		$E2$
$\frac{33}{2}^+$	$Z+3960.2$	667.9	25(2)	0.87(3)		$E2$
$\frac{37}{2}^+$	$Z+4703.6$	743.4	20(2)	0.89(8)		$E2$
$\frac{41}{2}^+$	$Z+5521.9$	818.3	20(2)	1.03(5)		$E2$
$(\frac{45}{2}^+)$	$Z+6415.1$	893.2	15(1)			$E2$
$(\frac{49}{2}^+)$	$Z+7395.3$	980.2	11(1)			$E2$
$(\frac{53}{2}^+)$	$Z+8471.4$	1076.1	7(1)			$E2$
$(\frac{57}{2}^+)$	$Z+9643.2$	1171.8	4(1)			$E2$
$(\frac{61}{2}^+)$	$Z+10903$	1259	<4			$E2$
$(\frac{65}{2}^+)$	$Z+12222$	1319	<4			$E2$
$(\frac{69}{2}^+)$	$Z+13576$	1354	<4			$E2$
	Band 4 : [402]5/2 $\alpha=-\frac{1}{2}$					
$\frac{7}{2}^+$	$Z+237.1$	146.1	38(13)	0.47(2)		$M1/E2$
$\frac{11}{2}^+$	$Z+629.4$	392.3	21(1)	1.09(9)	0.76(5)	$E2$
		213.7	29(2)	0.65(3)		$M1/E2$
$\frac{15}{2}^+$	$Z+1136.8$	507.4	30(2)	0.92(9)	1.45(9)	$E2$
		268.5	14(1)	0.57(5)		$M1/E2$
$\frac{19}{2}^+$	$Z+1730.2$	593.4	30(2)	1.1(1)	2.4(2)	$E2$
		311.0	8(1)			$M1/E2$
$\frac{23}{2}^+$	$Z+2378.9$	648.7	32(2)	1.0(1)	4.2(7)	$E2$
		344.8	9(1)			$M1/E2$
$(\frac{27}{2}^+)$	$Z+3053.5$	674.6	22(2)			$E2$
$(\frac{31}{2}^+)$	$Z+3712.6$	659.1	14(2)			$E2$
$(\frac{35}{2}^+)$	$Z+4413.1$	700.5	10(1)			$E2$
$(\frac{39}{2}^+)$	$Z+5192.5$	779.4	7(1)			$E2$
$(\frac{43}{2}^+)$	$Z+6078.9$	886.4	4(1)			$E2$
$(\frac{47}{2}^+)$	$Z+7078$	999	<4			$E2$
$(\frac{51}{2}^+)$	$Z+8178$	1100	<4			$E2$
$(\frac{55}{2}^+)$	$Z+9337$	1159	<4			$E2$

[a]Spin and parity of the initial state.
[b](X,Y,Z) are unknown constant energy values which should be added to the listed energy levels since the real excitation energies of the configurations are not known.
[c]Uncertainties in E_γ are 0.2 keV for most transitions, except for relatively weak transitions which are 0.5 keV.
[d]Relative intensity of the transition, where $I_\gamma(524.3)\equiv100$.
[e]The branching ratio $[=I(E2)/I(M1)]$ was extracted by gating above the level of interest.
[f]The intensity could not be determined.

and with the $N=69$ isotones ^{127}Ce [25,26] and ^{125}Ba [27,28].

A. Negative-parity structures

The identification of structures in ^{129}Nd was derived from the γ-γ-recoil data in the ORNL experiment. Figure 3(a)

shows a summed coincidence spectrum from a mass 129 gated γ-γ matrix. By examining the γ-charged particle matrix, we were also able to determine that the strongest and cleanest transitions in this band were associated with a $2p$ evaporation. This additional information allows for the structure to be unequivocally associated with ^{129}Nd, as it is the
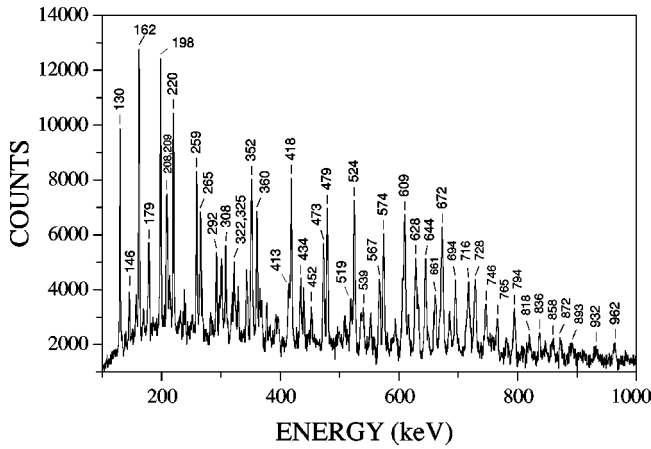
FIG. 2. Transitions from $A = 129$ recoils in the ORNL experiment. Transitions in coincidence with three protons and $A = 129$ (^{129}Pr) were subtracted, leaving ^{129}Nd γ rays (see text for details).
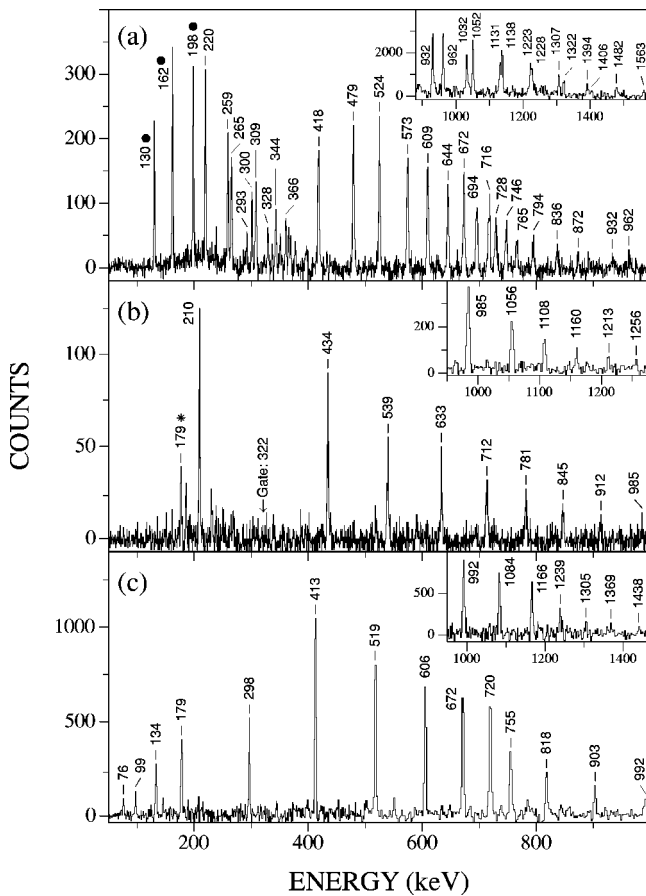
FIG. 3. Spectra of the negative-parity configurations: (a) both signatures of band 1, and (b) $\alpha = +\frac{1}{2}$ and (c) $\alpha = -\frac{1}{2}$ of band 2. The main spectra in panels (a) and (b) are ORNL mass-gated spectra. The main spectrum in panel (a) is produced from the sum of the individual gated spectra of the peaks denoted by a filled circle. The spectrum produced in the main panel (c) and all the insets in the figure are the the sum of many double-gated coincidence spectra from Gammasphere data. Peaks denoted by * are associated with γ rays from signature partners.

only $A = 129$ nucleus which can be produced by the emission of two protons. This confirms the preliminary results reported by Watson *et al.* [15], where this same band was observed up to a spin of $\frac{39}{2}$. In Ref. [15], mass-gating techniques similar to those described above were used, but without a charged-particle detector. This structure has been extended up to spin $\frac{75}{2}$ from the Gammasphere data [see the inset of Fig. 3(a)], and is the most intensely populated sequence in ^{129}Nd. The in-band properties [alignments and $B(M1)/B(E2)$ ratios] indicate a negative-parity configuration and this band is likely built on the $\frac{7}{2}^-$ isomeric state observed in Ref. [24]. The yrast sequence in ^{125}Ba, ^{127}Ce, and ^{131}Nd also have $\frac{7}{2}^-$ band-head states, which is consistent with our assignment.

A second sequence of transitions was identified in the $A = 129$ matrix, and is shown in Fig. 3(b). Similar to band 1, the strongest transitions were associated with the $2p$ channel. Thus this new structure can also be firmly assigned to ^{129}Nd, even though no linking transitions were observed. The Gammasphere data allowed for an extension of the sequence up to $I = \frac{71}{2}$, as seen in the inset of Fig. 3(b) and in Fig. 1, where the structure is labeled band 2. Additionally, the signature partner of band 2 was identified in the Gammasphere data, and a representative spectrum is displayed in Fig. 3(c). From Fig. 1, one may note that band 2 is not strongly coupled, with one signature lying lower in energy than its partner. An analysis of the in-band properties (e.g., alignment and signature splitting; see below) of band 2 indicates that a negative-parity assignment is appropriate, and the similarities with a structure in ^{131}Nd (where spins and parities are known) suggest a band-head spin of $\frac{1}{2}^-$ for band 2.

B. Positive-parity structures

The sequence displayed in Fig. 4(a) was observed in the ORNL data, and, in a similar manner to bands 1 and 2 discussed above, it was firmly assigned to ^{129}Nd. The structure is labeled band 3 in Fig. 1, and it was extended to $I = \frac{71}{2}$ from the Gammasphere data as shown in the inset of Fig. 4(a). A short sequence of transitions was also found in the Gammasphere data [see Fig. 4(b)], which was identified as the signature partner of band 3. In Fig. 1 one may note that the latter sequence lies much higher in excitation energy than its partner, which is why it could not be extended to higher spins. Band 3 has similar in-band properties, such as a low-K, positive-parity structure in ^{131}Nd, therefore, it has been assigned even parity and a band-head spin of $\frac{1}{2}^+$ [29].

A new strongly coupled band, which interacts with band 3 at low spins, was observed in the Gammasphere data. Spectra of both signatures are given in Figs. 4(c) and 4(d), and the band is labeled band 4 in Fig. 1. A DCO ratio of 0.43(6) was found for the 138.8-keV transition depopulating the $\frac{7}{2}^+$ state in band 3 to the band head of band 4, indicating a change in spin of $1\hbar$. The 482.6- and 589.2-keV linking transitions from band 4 to 3 were determined to have an $E2$ nature (see Table I), which establishes that bands 3 and 4 have the same parity and that the 138.8-keV transition must correspond to a $I \rightarrow I-1$ deexcitation. Therefore, a band-head spin of $\frac{5}{2}^+$ is assigned, which is consistent with the configuration (see be-
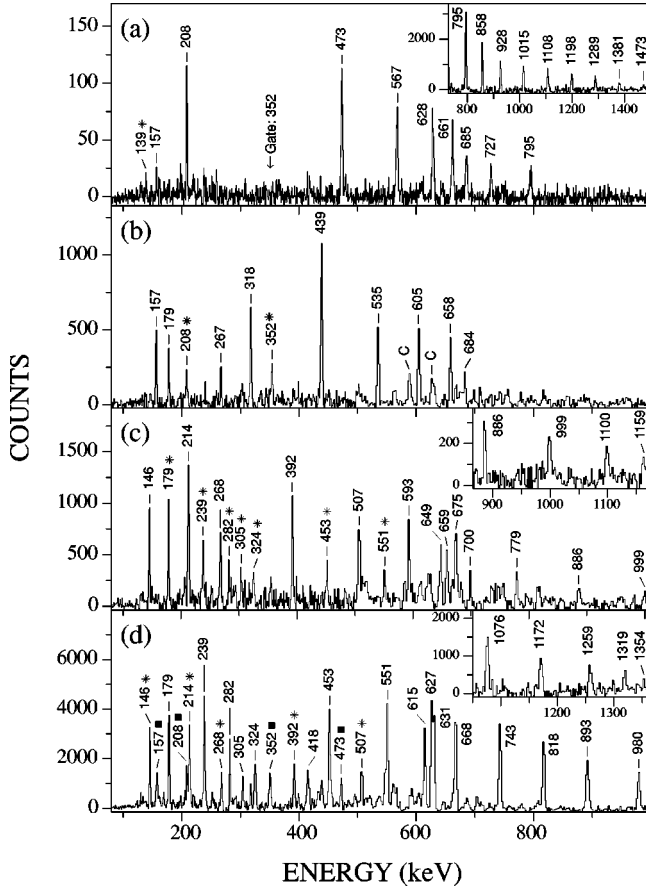
FIG. 4. Sample spectra of the positive-parity configurations: (a) $\alpha = -\frac{1}{2}$, (b) $\alpha = +\frac{1}{2}$ of band 3, and (c) $\alpha = -\frac{1}{2}$, (d) $\alpha = +\frac{1}{2}$ of band 4. The insets in panels (a), (c), and (d) and the spectra in main panels (b), (c), and (d) are the results of summing many double-gated coincidence spectra from Gammasphere data. The main spectrum in panel (a) is an ORNL mass-gated spectrum. Peaks denoted by * are associated with γ rays from signature partners, and peaks denoted by c are contaminant γ rays. Peaks denoted by filled squares in panel (d) belong to the [411]1/2 band.

low) and systematics observed for similar structures in ^{131}Nd and ^{127}Ce.

IV. CONFIGURATION ASSIGNMENTS

In order to help identify the active orbitals nearest to the Fermi surface at $N = 69$, we provide a neutron single-particle diagram in Fig. 5. Total Routhian surface (TRS) calculations [30] predicted a ground-state deformation near $\beta_2 = 0.305$ for ^{129}Nd. For a prolate deformation of this size, one can deduce from Fig. 5 that bands based on the $h_{11/2}[523]7/2$, $d_{3/2}[411]1/2$, $d_{5/2}[402]5/2$, and $(h_{9/2}/f_{7/2})[541]1/2$ orbitals should be observed at relatively low excitation energies. Band characteristics such as the alignment behavior, the $B(M1)/B(E2)$ ratios, and the signature splitting were considered to associate the observed bands in ^{129}Nd with the orbitals mentioned above.

A. Alignments and band crossings

The alignments of the bands in ^{129}Nd are plotted versus rotational frequency in Fig. 6. Harris parameters [31] of $\mathcal{J}_0$

$= 22~\hbar^2/\text{MeV}$ and $\mathcal{J}_1 = 17~\hbar^4/\text{MeV}^3$ were used to subtract the angular momentum of the collective core. The observed crossings are labeled in Fig. 6 using the standard alphabetic quasiparticle labeling scheme [32], which is summarized in Table II in terms of the orbital's parity, signature (π, α), and configuration at zero rotational frequency.
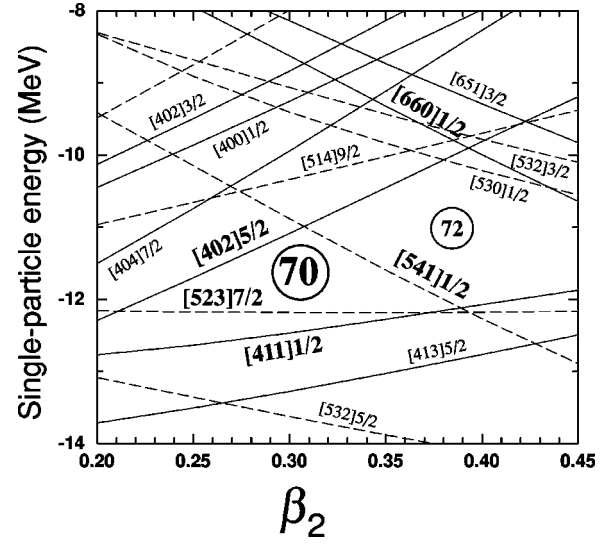
FIG. 5. Neutron single-particle levels as a function of quadru-pole deformation (where $\beta_4 = 0$ and $\gamma = 0°$) calculated using the Woods-Saxon potential [42] with parameters given in Ref. [43].

1. Negative-parity structures

Watson *et al.* [15] suggested that band 1 is based upon an $\nu h_{11/2}$ orbital, but due to limited information, they were not able to propose a definitive configuration. The band under-
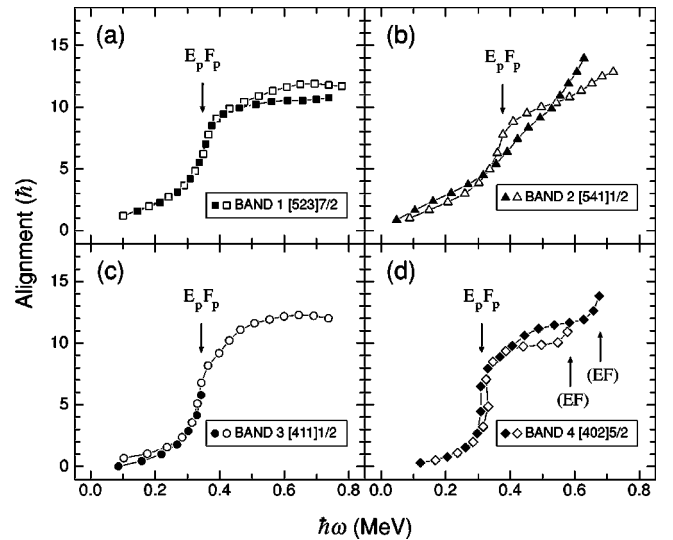
FIG. 6. The alignment plotted vs rotational frequency for bands 1–4. Harris parameters of $\mathcal{J}_0 = 22~\hbar^2/\text{MeV}$ and $\mathcal{J}_1 = 17~\hbar^4/\text{MeV}^3$ were used to subtract the angular momentum of the collective core. The positive and negative signatures are denoted by filled and open symbols, respectively. Proposed band-head configurations are also given in the legends.

TABLE II. Alphabetic quasiparticle labeling scheme for ^{129}Nd.

Label	$(\pi,\alpha)_n$ [a]	Configuration [b]	Label	$(\pi,\alpha)_n$ [a]	Configuration [b]
		Quasineutrons			
A	$(+,+\frac{1}{2})_1$	$[411]1/2$	B	$(+,-\frac{1}{2})_1$	$[411]1/2$
C	$(+,+\frac{1}{2})_2$	$[402]5/2$	D	$(+,-\frac{1}{2})_2$	$[402]5/2$
E	$(-,-\frac{1}{2})_1$	$[523]7/2$	F	$(-,+\frac{1}{2})_1$	$[523]7/2$
G	$(-,-\frac{1}{2})_2$	$[541]1/2$	H	$(-,+\frac{1}{2})_2$	$[541]1/2$
		Quasiprotons			
E_p	$(-,-\frac{1}{2})_1$	$h_{11/2}$	F_p	$(-,+\frac{1}{2})_1$	$h_{11/2}$

[a]Parity (π) and signature (α) of the orbital. The subscript n numbers the quasiparticle's excitations of a specific signature and parity starting with the lowest in energy at $\hbar\omega=0$ MeV.
[b]Configuration of the orbital at $\hbar\omega=0$ MeV.

goes an alignment at $\hbar\omega_c\sim0.35$ MeV, and has an alignment gain of $\Delta i\sim9\hbar$. The only quasiparticles near the Fermi surface that can align at this low frequency and produce the large alignment gain are the lowest $h_{11/2}$ quasiprotons (E_p and F_p). The E_pF_p band crossing is well known in the mass 130 region, and the alignment gain and crossing frequency are consistent with the first proton crossings observed in other $A\sim130$ nuclei. Cranked shell-model (CSM) [33] calculations for the protons and neutrons in ^{129}Nd were performed using the deformation parameters taken from a TRS calculation for the E and F neutron configurations at a frequency of $\hbar\omega\sim0.30$ MeV. A predicted E_pF_p crossing occurs at $\hbar\omega_c\sim0.36$ MeV, which is in good agreement with the first observed crossing in band 1. In the quasineutron diagram, shown in Fig. 7, the first neutron crossing is predicted to occur at $\hbar\omega_c\sim0.49$ MeV, but no crossings are

FIG. 7. Cranked shell model calculation for quasineutrons in ^{129}Nd. The deformation parameters (shown at the top of the figure) were determined from TRS calculations. Interpretation of the lines is displayed at the top of the figure. An explanation of the orbital labeling scheme is given in Table II.

experimentally observed up to high frequencies of ~0.8 MeV. The blocking of this crossing implies that band 1 is based upon a $\nu h_{11/2}$ orbital, which is most likely $[523]7/2$ as it is the nearest $\nu h_{11/2}$ orbital to the ^{129}Nd Fermi surface (see Fig. 5). Thus the negative-parity and band-head spin assignments shown in Fig. 1 are consistent with similar bands in nearby nuclei. The CSM predicts two other neutron crossings, i.e., FG and EH crossings at ~0.6 MeV as seen in Fig. 7; however neither crossing is observed in band 1. This behavior is contrary to ^{131}Nd where both of these crossings are observed near the predicted CSM frequency of ~0.6 MeV [22]. These crossings may be delayed in a manner similar to the delayed EF crossings observed in even-even Ce nuclei [34–36], and in other bands in ^{129}Nd (see below).

As seen from Fig. 6(a), the negative signature of band 1 has $\sim1-2$ $\hbar$ more alignment than its signature partner after the proton alignment. The small magnitude of this alignment indicates that it is not likely due to the FG crossing, as $4-5$ $\hbar$ has been associated with this alignment in nearby nuclei. TRS calculations were done for both signatures of the $\nu h_{11/2}$ configuration in ^{129}Nd for the frequency range $(0.24-0.59$ MeV) in order to test whether signature-dependent deformation effects can account for this behavior. However, the calculations show little difference in potential depth or quadrupole deformation between the two signatures over the frequency range, indicating that this gain of alignment is likely not due to different deformations. The cause(s) of this interaction is not clear at this time.

Band 2 is associated with a low-K configuration as large signature splitting is initially observed (see Fig. 1). The gradual increase of alignment at low frequency is similar to that observed in the $[541]1/2$ bands of ^{131,133}Nd [10,22]. Also, the apparent differing interaction strengths in the E_pF_p crossing region are strikingly similar to those seen in the $\nu h_{9/2}/f_{7/2}$ bands of ^{131,133}Nd; therefore, band 2 is assigned the $[541]1/2$ configuration. Rotational bands based on this orbital are known to have an intermediate deformation (between normal and highly deformed) [4]; thus the chosen Harris parameters may be less appropriate for band 2 causing the gradual increase of alignment at low frequency seen in Fig.
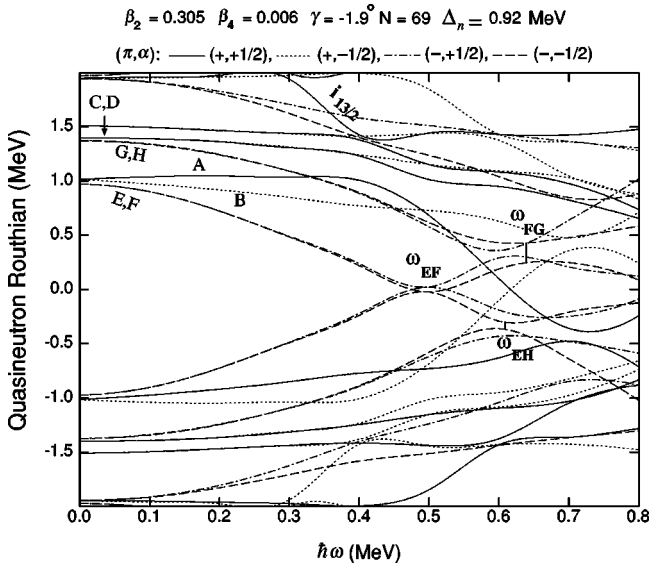
6. The differing interaction strengths in the $E_p F_p$ crossing region are unusual, as no such signature-dependent behavior is observed in the other ^{129}Nd bands. Perhaps another three-quasiparticle band based on the [530]1/2⊗ $E_p F_p$ configuration crosses the negative signature sequence as it undergoes the proton alignment, as addressed previously in Ref. [22]. A crossing is observed near 0.54 MeV in the positive signature, while the negative signature shows a crossing near 0.65 MeV. The next possible proton crossing is not predicted to occur until very high frequencies ($\hbar\omega > 1$ MeV); therefore, this second crossing is likely the result of a pair of neutrons aligning. The EF crossing is predicted to occur near 0.5 MeV (see Fig. 7); however, one would expect both signatures of the [541]1/2 band to experience this neutron alignment at approximately the same frequency. Therefore, an interpretation of these crossings is at present lacking.

2. Positive-parity structures

In Fig. 6(c), a large gain in alignment ($\Delta i \sim 9\hbar$) can be observed at a crossing frequency of $\hbar\omega_c \approx 0.33$ MeV for the favored signature ($\alpha = -\frac{1}{2}$) of band 3. Once again, the $h_{11/2}$ quasiproton alignment is responsible for this gain. This structure exhibits a significant amount of signature splitting at lower spin (see Fig. 1) indicating that it likely corresponds to a low-K sequence. As stated previously, bands 3 and 4 have the same parity; from arguments given below, band 4 most likely has positive parity. An inspection of Fig. 5 indicates that the nearest positive-parity, low-K orbital is the [411]1/2 level; thus band 3 is assigned to this configuration. A second alignment in band 3 occurs near 0.43 MeV, inducing a gain of $\sim 2-3$ $\hbar$. While it is possible this is the EF crossing, it appears to be at a crossing frequency lower than expected by CSM calculations and much lower than that observed in band 4 (see below). The EF crossing is also known to be delayed in this region, rather than to occur at lower than expected frequencies [34]. Perhaps this is a crossing with a "more deformed," band seen at $\hbar\omega \sim 0.2$ MeV in the [411]1/2 band of ^{131}Nd. The more deformed sequence is caused by a pair of neutrons scattering into the deformation driving [541]1/2 orbital. Once again, similar to ^{131}Nd, the [411]1/2 band is the only sequence to experience this crossing, which Hartley *et al.* [22] suggested to be a result of blocking and Fermi-level position effects for the other bands. The higher crossing frequency in ^{129}Nd as compared with ^{131}Nd is due to the [541]1/2 orbital likely lying higher in energy for the former nucleus.

The lack of signature splitting in band 4 (up to spin $\frac{23}{2}$), as shown in Fig. 1, suggests a configuration with high K. The [402]5/2 and [413]5/2 orbitals are possible candidates, but the $B(M1)/B(E2)$ ratios, discussed in Sec. V, clearly indicate that band 4 should be associated with the [402]5/2 orbital. This assignment is consistent with a similar structure found in the $^{127}_{58}$Ce [25] isotone and in ^{131}Nd. Wilmarth *et al.* [23] suggested an $I^\pi = (\frac{5}{2}^+)$ assignment for the ground state of ^{129}Nd. If this is correct, we can rule out the possibility that the ground state is based on the [402]5/2 configuration, since the [402]5/2 band lies higher in energy relative to the [411]1/2, orbital as seen in Fig. 1. Inspection of Fig. 5, as

well as the observed intensities, indicates that the [411]1/2 and the [523]7/2 orbitals are much closer to the Fermi surface than any other $K = \frac{5}{2}$ state. Therefore, either the $\frac{1}{2}^+$ or the $\frac{7}{2}^-$ state from bands 3 and 1, respectively, should also be considered as possible candidates for the ground state of ^{129}Nd.

The alignment of the negative signature of band 4, shown in Fig. 6(d), indicates that the sequence undergoes an $E_p F_p$ crossing at $\hbar\omega_c \approx 0.31$ MeV. The upbend near 0.6 MeV is likely the EF neutron crossing. An additional gain of $\sim 2\hbar$ in alignment occurs in the positive signature after the proton alignment, as compared with the negative signature, at $\hbar\omega_c \sim 0.43$ MeV. A crossing with a more deformed band, as seen in band 3, is unlikely since both signatures would be expected to experience an alignment gain. Instead, an adiabatic crossing with the $\nu i_{13/2}$ orbital may cause the additional alignment gain in the positive signature of band 4. This is reminiscent of an $i_{13/2}$ crossing in ^{131}Nd [22] and ^{135}Sm [37]. The occupation of the $i_{13/2}$ neutron intruder orbitals is known to be a prominent factor in driving the nuclear shape toward higher deformation for nuclei in the $A \sim 130$ region [4,8]. By inspecting the CSM calculations in Fig. 7, one can see that the $\nu i_{13/2}$ [660]1/2 intruder orbital interacts with the C configuration (the [402]5/2 orbital) at $\hbar\omega_c \sim 0.43$ MeV, which is remarkably consistent with the experimental observations. The alignment gain near 0.7 MeV is likely the EF crossing, which is delayed in comparison with observations in the negative signature. Such a delay is consistent with the positive signature having a larger deformation due to the exchange of character from $d_{5/2}$ to $i_{13/2}$. Thus there is evidence to suggest the observation of the intruder $i_{13/2}$ orbital; however, further experimental verification of the larger deformation is required to confirm the assignment.

B. $B(M1)/B(E2)$ transition strength ratios

Experimental $B(M1)/B(E2)$ ratios were extracted using the observed γ-ray energies and branching ratios [$\lambda = I_\gamma(I \rightarrow I-2)/I_\gamma(I \rightarrow I-1)$] according to the standard formula [27]

$$\frac{B(M1:I \rightarrow I-1)}{B(E2:I \rightarrow I-2)} = 0.693 \frac{E_\gamma^5(I \rightarrow I-2)}{E_\gamma^3(I \rightarrow I-1)} \times \frac{1}{\lambda(1+\delta^2)} \left(\frac{\mu_N}{e\mathrm{b}}\right)^2,$$

where E_γ is in MeV. To determine the magnitude of the mixing ratios δ for the $\Delta I = 1$ transitions, rotational model calculations [38] were performed using the measured branching ratios and assuming pure K. The resulting $B(M1)/B(E2)$ ratios are plotted in Fig. 8 along with theoretical predictions for possible configurations.

Theoretical calculations of $B(M1)/B(E2)$ ratios were performed with the rotational model form of the $B(E2)$ transition strength [38], and an extended formalism [39] of the geometrical model from Dönau [40] and Frauendorf [41] to determine the $B(M1)$ strength. An intrinsic quadrupole moment of $Q_0 = 5.32e$b was assumed for ^{129}Nd from TRS calculations. While the collective gyromagnetic ratio was given by $g_R = Z/A$, the g_K values were calculated using a Woods-Saxon potential [42], with the following results
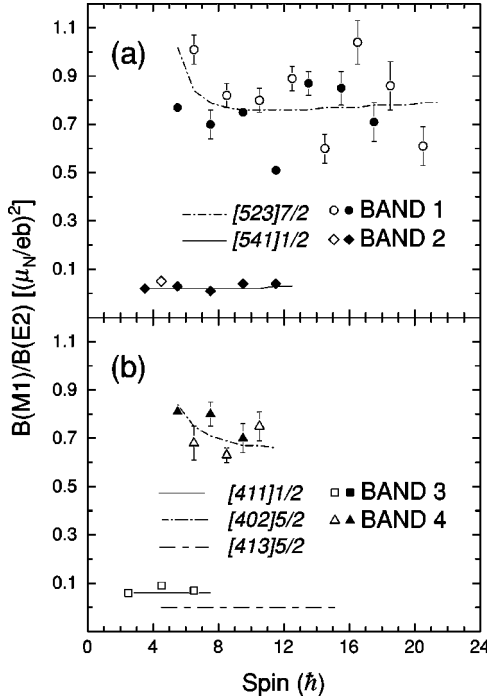
FIG. 8. The experimental (symbols) and theoretical (lines) $B(M1)/B(E2)$ ratios for (a) bands 1 and 2 and (b) bands 3 and 4. The positive and negative signatures are denoted by filled and open symbols, respectively.

for the possible active orbitals shown in Fig. 5: $g_K([402]5/2) = -0.49$, $g_K([413]5/2) = 0.40$, $g_K([411]1/2) = 1.90$, $g_K([523]7/2) = -0.32$, and $g_K([541]1/2) = -0.54$.

The $B(M1)/B(E2)$ ratios for the negative- and positive-parity configurations are shown in Figs. 8(a) and 8(b), respectively. Arguments were previously given that band 1 is based upon an $h_{11/2}$ neutron, and a good fit is found for the $B(M1)/B(E2)$ ratios with the predicted $[523]7/2$ values. A good agreement is observed between the experimental values for band 3 and the theoretical calculations for the $[402]5/2$ orbital. The calculated values for the $[413]5/2$ configuration are an order of magnitude lower than those found for band 3, so this configuration can be confidently ruled out. Bands 2 and 4 have small $B(M1)/B(E2)$ ratios, as shown in Figs. 8(a) and 8(b), which is expected for low-K structures. Good agreement between the calculated and observed ratios is found for our assignments of bands 2 and 4 as the $[411]1/2$ and $[541]1/2$ structures, respectively.

V. SIGNATURE SPLITTING SYSTEMATICS OF THE $\nu h_{11/2}$ BANDS IN ODD-$A \sim 130$ NUCLEI

Signature is the symmetry quantum number related to the invariance of a nucleonic state under a rotation by 180° about the rotation axis. Odd-A nuclei possess two values of the signature (α) according to the equation $\alpha_I = \frac{1}{2}(-1)^{I-1/2}$, where I is the spin of a given state. Similarly, the energetically favored signature of a coupled band can be determined by $\alpha_f = \frac{1}{2}(-1)^{j-1/2}$. Therefore, in the $\nu h_{11/2}$ bands, the $\alpha = -\frac{1}{2}$ signature is expected to be favored. The

degree of signature splitting in a band usually relates to the admixture of the $K = \frac{1}{2}$ component in its wave function, which has a decoupling parameter [38] separating the two signatures. Therefore, a small signature splitting is expected in mid- to high-K orbitals, where only a small component of $K = \frac{1}{2}$ is expected. However, a large signature splitting was observed in $K = (\frac{7}{2}, \frac{9}{2})$ $\pi h_{11/2}$ bands in $N \sim 90$ ($A \sim 160$) nuclei [44], and this was suggested to be the result of negative triaxial deformations [45]. While high-K orbitals tend to drive the soft nuclear core toward oblate shapes, the core "prefers" a prolate deformation. These two opposing forces can create stable triaxial shapes [11]. A large signature splitting in the $A \sim 130$ region is also observed as the analogous neutron $h_{11/2}$ orbitals are occupied. In our analysis, we investigate the degree of triaxiality needed to achieve the energy splitting within the framework of the CSM, and define any observed trends.

The signature splitting of the energy levels for the proton rich Ba-Ce-Nd-Sm nuclei is displayed in Fig. 9. Data for the nuclei, other than ^{129}Nd, were compiled from the following sources: ^{123}Ba [46], ^{125}Ba [29], ^{127}Ba [47], ^{129}Ba [48], ^{131}Ba [49], ^{125}Ce [50], ^{127}Ce [25], ^{129}Ce [51], ^{131}Ce [52], ^{133}Ce [53], ^{131}Nd [22], ^{133}Nd [54], ^{135}Nd [55], ^{133}Sm [56], ^{135}Sm [37], and ^{137}Sm [57]. The convention $[E(I)-E(I-1)]/2I$ was used to display the energy splitting, where $E(I)$ is the energy of a state with spin I. For discussion purposes, the calculated quadrupole deformation (β_2) from Ref. [14] is given in Fig. 9 for each nucleus. The large region of deformation covered by these nuclei varying from $N = 67$ ($K = \frac{7}{2}$) to 75 ($K = \frac{9}{2}$), will reveal the signature splitting dependence on β_2 and on the neutron Fermi surface.

A. Low-spin region $I < \frac{27}{2}$

As seen from Fig. 9, two general trends are observed.

(1) The signature splitting *increases* with N for a given isotopic chain. This is contrary to what is expected if only Coriolis coupling is involved, as K increases with N. It is also seen that β_2 *decreases* with N, which is related to the proximity of the $N = 82$ spherical shell gap.

(2) The signature splitting *increases* as Z decreases in a given isotone chain, while β_2 *decreases* along the chain due to the $Z = 50$ shell gap.

The decrease in β_2 deformation makes the nuclei more susceptible to the oblate-driving forces of the high-K, $\nu h_{11/2}$ orbitals, and this can produce a γ deformation. The signature splitting dependence on γ and β_2 can be investigated within the CSM to reveal which type of deformation plays the dominant role. The nucleus ^{129}Ba was used as an example, since a large splitting was observed for the expected high-$K(\frac{9}{2})$ $\nu h_{11/2}$ band. The results of our calculations are presented in Fig. 10, where one can see that the experimental energy difference in the Routhian $(\Delta e')$ is 200 keV at a frequency of 0.3 MeV. If a small amount of γ deformation is assumed and held constant, the signature splitting does increase with decreasing β_2 (Fig. 10). However, unrealistically low β_2 values must be used to reproduce the experimentally observed splitting in ^{129}Ba, implying that β_2 alone cannot
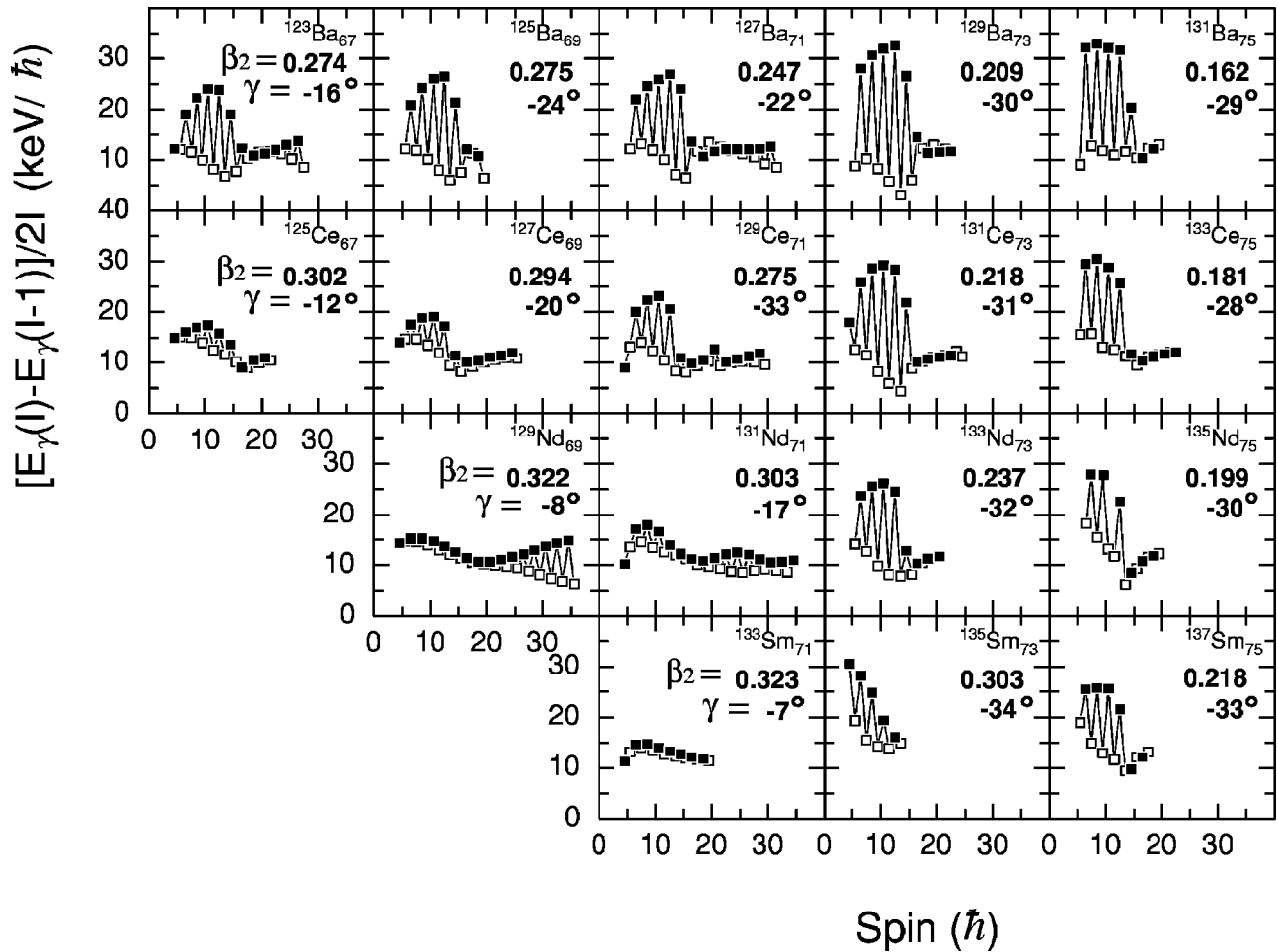
FIG. 9. Signature splitting for the $\nu h_{11/2}$ bands as a function of spin in odd-A Ba ($Z=56$), Ce ($Z=58$), Nd ($Z=60$), and Sm ($Z=62$) nuclei. The $\alpha=+\frac{1}{2}$ ($\alpha=-\frac{1}{2}$) signature is denoted by filled (open) squares. K values of $\frac{7}{2}$ and $\frac{9}{2}$ for the $\nu h_{11/2}$ bands are assumed for $N=67-71$ and $N=73-75$, respectively. The quadrupole deformation (β_2) shown for each of the nuclei is taken from Ref. [14]. The γ deformation values shown are evaluated from the CSM as discussed in the text.
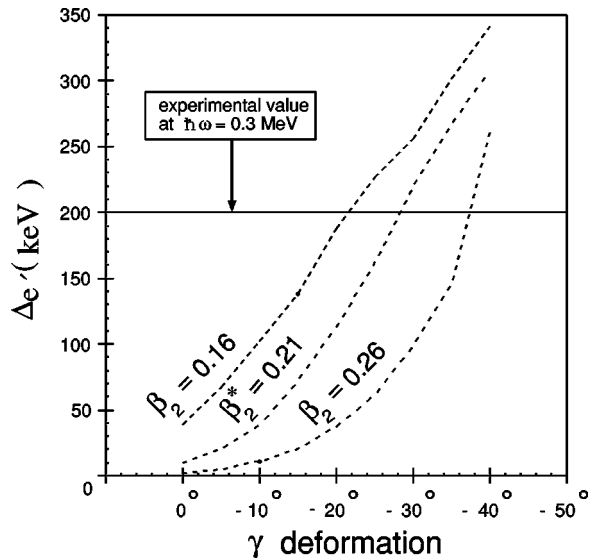
FIG. 10. Theoretical CSM calculations of sinature splitting in the $\nu h_{11/2}$ band vs γ deformation for ^{129}Ba. The calculations were carried out for three different β_2 values at $\hbar\omega=0.30$ MeV. The β_2 value denoted by a * is taken from Ref. [14].

describe the splitting. The experimentally observed splitting can be reproduced using the predicted quadrupole deformation from Möller *et al.* [14], $\beta_2=0.21$, and a reasonable γ value of $-28°$. The experimental crossing frequency can also be reproduced for $\beta_2=0.16$ and 0.26 using γ values of $\sim-20°$ and $\sim-36°$, respectively. Therefore, appreciable triaxial deformations appear to be a crucial parameter in CSM calculations in order to reproduce the unusually large splitting in ^{129}Ba.

Using β_2 values from Ref. [14], we performed CSM calculations in a similar manner for every nucleus in Fig. 9 in order to investigate the magnitude and the trends in γ deformation. The derived values for the triaxial deformation are shown in Fig. 9. A range of negative γ values was found, from $\gamma\sim-10°$ in the lightest nuclei to $\gamma\sim-30°$ in the heaviest. The amount of γ deformation generally increases with N along an isotopic chain, which corresponds to an increase in the observed signature splitting and decrease in β_2. The γ deformation decreases with increasing Z along an isotonic chain, which corresponds to a decrease in the observed signature splitting and increase in β_2. The more neutron-deficient nuclei generally have small γ deformation,

as well-deformed, prolate minima are expected. TRS calculations by Granderath *et al.* [11] also showed a significant increase in negative γ deformation with increasing N for the $\nu h_{11/2}$ configurations in Xe-Ba-Ce isotope chains. However, their calculations suggested that extremely large γ values of $\sim -70°$ were necessary to reproduce the signature splitting of the heavier nuclei. In contrast, the CSM predicts more modest triaxial deformation values that can also explain the large signature splitting.

B. High-spin region $I > \frac{27}{2}$

All of the $\nu h_{11/2}$ bands in Fig. 9 show a distinctive band crossing at $I \sim 15$, which is due to the alignment of two low-K $h_{11/2}$ protons. Although signature splitting is present at lower spins ($I < \frac{35}{2}$), it is greatly reduced above the crossing. Since signature splitting is a sensitive probe of the deformation, this can be taken as an indication that the three-quasiparticle band above the band crossing has a different deformation than the one quasiparticle band below it. The low-K protons tend to drive the nucleus toward prolate ($\gamma = 0°$) shapes in contrast to the high-K neutrons [11]. The much smaller energy splitting found in the $\pi h_{11/2} \nu h_{11/2}$ bands of neighboring odd-odd nuclei [58] suggest that the deformation driving force of the proton is greater than that of the neutron. Thus, after the proton alignment in the $\nu h_{11/2}$ bands of the odd-A nuclei, the triaxial deformation may indeed change and have a value closer to $\gamma \sim 0°$. This is a behavior similar to that seen in $A \sim 160$ region, where the splitting is quenched after the alignment of low-K $i_{13/2}$ neutrons.

Not only is the splitting reduced after the $\nu i_{13/2}$ alignment in the $A \sim 160$ nuclei, but in many cases the normally unfavored signature lies lower in energy above the crossing. This phenomenon is known as signature inversion, and is also seen in the $\pi h_{11/2} \nu h_{11/2}$ bands of the odd-odd $A \sim 130$ nuclei [58]. The cause of the inversion in the $\pi h_{11/2} \nu (i_{13/2})^2$ structures has been suggested to lie in the $i_{13/2}$ neutron driving the shape of the nucleus to a small, positive γ value [59]. Signature inversion is also seen in the $\nu h_{11/2}$ bands of ^{123,127,129,131}Ba, ^{131,133}Ce, ^{135}Nd, and ^{137}Sm after the proton crossing, as seen in Fig. 9. While the inversion lasts for a large spin range in $A \sim 160$ nuclei, normal ordering of the signatures is restored within a few units of spin for the $\nu h_{11/2}$ bands in $A \sim 130$ nuclei. This suggests that the normal Coriolis effects supersede the force responsible for inversion at higher spins and, thus, that this force is weaker in the $A \sim 130$ nuclei as compared with the $A \sim 160$ region.

The change in shape from negative γ deformation before the crossing to positive γ deformation after the crossing may be the cause for the observed signature inversion in $A \sim 130$ nuclei. However, the role of a p-n interaction may also need to be considered as there is evidence to suggest that it is the cause of inversion in nearby odd-odd nuclei [60]. Clearly, theoretical work is needed to fully understand this inversion process.

VI. CONCLUSIONS

In summary, progress toward discrete γ-ray spectroscopy near the proton drip line has been made in odd-A neodymium nuclei, as over 140 transitions have been placed in the level scheme of ^{129}Nd for the first time and assigned to four different structures. The selectivity of the RMS and the charged-particle array HyBall in combination with the CLARION Ge array at ORNL, as well as the power of Gammasphere in conjuction with the Microball, was used to positively identify the structures. Several quasiparticle alignments were observed in the bands, which were interpreted within the cranked shell model. Evidence of the identification of the $\nu i_{13/2}$ band was presented as it appears to adiabatically cross the [402]5/2 configuration. A systematic study of signature splitting in the $\nu h_{11/2}$ bands was performed for the mass $A \sim 130$ proton-rich nuclei. The trends in the splitting are explained as a manifestation of γ deformation at low spin, and a comparison was made with the mass $A \sim 160$ region where similar trends are observed. This comparison appears to further strengthen the role of triaxiality in $A \sim 130$ nuclei.

[1] D.B. Fossan, J.R. Hughes, Y. Lian, R. Ma, E.S. Paul, and N. Xu, Nucl. Phys. **A520**, 241c (1990).

[2] R.M. Clark *et al.*, Phys. Rev. Lett. **76**, 3510 (1996).

[3] B.H. Smith, L.L. Riedinger, H.Q. Jin, W. Reviol, W. Satula, A. Galindo-Uribarri, D.G. Sarantites, J.N. Wilson, D. LaFosse, and S.M. Mullins, Phys. Lett. B **443**, 89 (1998).

[4] F.G. Kondev *et al.*, Phys. Rev. C **60**, 011303(R) (1999).

[5] C.M. Petrache, D. Bazzacco, S. Lunardi, C. Rossi Alvarez, R. Venturelli, R. Burch, P. Pavan, G. Maron, D.R. Napoli, L.H. Zhu, and R. Wyss, Phys. Lett. B **387**, 31 (1996).

[6] A. Galindo-Uribarri, D. Ward, H.R. Andrews, G.C. Ball, D.C. Radford, V.P. Janzen, S.M. Mullins, J.C. Waddington, A.V. Afanasjev, and I. Ragnarsson, Phys. Rev. C **54**, 1057 (1996).

[7] N.J. O'Brien *et al.*, Phys. Rev. C **58**, 3212 (1998).

[8] R. Wyss, J. Nyberg, A. Johnson, R. Bengtsson, and W. Nazarewicz, Phys. Lett. B **215**, 211 (1988).

[9] A.V. Afanasjev and I. Ragnarsson, Nucl. Phys. **A608**, 176 (1996).

[10] D. Bazzacco *et al.*, Phys. Rev. C **58**, 2002 (1998).

[11] A. Granderath, P.F Mantica, R. Bengtsson, R. Wyss, P. von Brentano, A. Gelberg, and F. Seiffert, Nucl. Phys. **A597**, 427 (1996).

[12] R.V.F. Janssens and F. Stephens, Nucl. Phys. News **6**, 9 (1996).

[13] D.G. Sarantites, P.-F. Hua, M. Devlin, L.G. Sobotka, J. Elson, J.T. Hood, D.R. LaFosse, J.E. Sarantites, and M.R. Maier, Nucl. Instrum. Methods Phys. Res. A **381**, 418 (1996).

[14] P. Möller, J.R. Nix, W.D. Myers, and W.J. Swiatecki, Acta Math. **59**, 185 (1995).

[15] D. C. B. Watson, A. N. James, M. A. Skelton, and J. Simpson, Liverpool University, annual report 1987–1988, 1989, p. 31.

[16] C.J. Gross et al., Nucl. Instrum. Methods Phys. Res. A **450**, 12 (2000).

[17] C.J. Gross, Z. Phys. A **358**, 249 (1997).

[18] J. D. Cole, T. M. Cormier, J. H. Hamilton, and A. V. Ramayya, Nucl. Instrum. Methods Phys. Res. **70**, 343 (1992).

[19] C. J. Gross, T. N. Ginter, Y. A. Akovali, M. J. Brinkman, J. W. Johnson, J. Mas, J. W. McConnell, W. T. Milner, D. Shapira, and A. N. James, in *CP392, Application of Accelerators in Research and Industry*, edited by J. L. Duggan and I. L. Morgan (AIP, New York, 1997), p. 401.

[20] D.C. Radford, Nucl. Instrum. Methods Phys. Res. A **361**, 297 (1995).

[21] W. Reisdorf, Z. Phys. A **300**, 227 (1981).

[22] D.J. Hartley et al., Phys. Rev. C **61**, 044328 (2000).

[23] P.A. Wilmarth et al., Z. Phys. A **321**, 179 (1985).

[24] A. Gizon et al., Z. Phys. A **358**, 369 (1997).

[25] B.M. Nyakó, J. Gizon, V. Barci, A. Gizon, S. André, D. Barnéoud, J. Genevey, and J.C. Merdinger, Z. Phys. A **334**, 513 (1989).

[26] J. Genevey et al., Z. Phys. A **356**, 7 (1996).

[27] R. Ma, E.S. Paul, S. Shi, C.W. Beausang, Jr., W.F. Piel, N. Xu, D.B. Fossan, T. Chapuran, D.P. Balamuth, and J.W. Arrison, Phys. Rev. C **37**, 1926 (1988).

[28] J. Katakura, Nucl. Data Sheets **86**, 955 (1999).

[29] J.P. Martin, V. Barci, H. El-Samman, A. Gizon, W. Klamra, B.M. Nyakó, F.A. Beck, Th. Byrski, and J.C. Merdinger, Nucl. Phys. **A489**, 169 (1988).

[30] W. Nazarewicz, G.A. Leander, and J. Dudek, Nucl. Phys. **A467**, 437 (1985).

[31] S.M. Harris, Phys. Rev. **138**, B509 (1965).

[32] R. Bengtsson, S. Frauendorf, and F.-R. May, At. Data Nucl. Data Tables **35**, 15 (1986).

[33] R. Bengtsson and S. Frauendorf, Nucl. Phys. **A327**, 139 (1979); **A314**, 27 (1979).

[34] E.S. Paul et al., Nucl. Phys. **A676**, 32 (2000).

[35] A.T. Semple, E.S. Paul, A.J. Boston, I.M. Hibbert, D.T. Joss, P.J. Nolan, N.J. ÓBrien, C.M. Parry, S.L. Shepherd, R. Wadsworth, and R. Wyss, J. Phys. G **24**, 1125 (1998).

[36] E.S. Paul et al., Nucl. Phys. **A619**, 177 (1997).

[37] S.M. Mullins et al., J. Phys. G **13**, L201 (1987).

[38] A. Bohr and B. R. Mottelson, *Nuclear Structure* (Benjamin, New York, 1975), Vol. 2.

[39] V.P. Janzen et al., Phys. Rev. C **45**, 613 (1992).

[40] F. Dönau, Nucl. Phys. **A471**, 469 (1987).

[41] S. Frauendorf, Phys. Lett. **100B**, 219 (1981).

[42] S. Ćwiok, J. Dudek, W. Nazarewicz, J. Skalski, and T. Werner, Comput. Phys. Commun. **46**, 379 (1987); J. Dudek, A. Majhofer, J. Skalski, T. Werner, S. Ćwiok, and W. Nazarewicz, J. Phys. G **5**, 1359 (1979).

[43] W. Nazarewicz, M.A. Riley, and J.D. Garrett, Nucl. Phys. **A512**, 61 (1990).

[44] D.J. Hartley, T.B. Brown, F.G. Kondev, J. Pfohl, M.A. Riley, S.M. Fischer, R.V.F. Janssens, D.T. Nisius, P. Fallon, W.C. Ma, and J. Simpson, Phys. Rev. C **58**, 2720 (1998).

[45] I. Hamamoto, Nucl. Phys. **A520**, 297c (1990).

[46] R. Wyss, F. Lidén, J. Nyberg, A. Johnson, D.J.G. Love, A.H. Nelson, D.W. Banes, J. Simpson, A. Kirwan, and R. Bengtsson, Z. Phys. A **330**, 123 (1988).

[47] A. Dewald et al., Eur. Phys. J. A **A3**, 103 (1998).

[48] K. Schiffer, A.P. Byrne, A.M. Baxter, G.D. Dracoulis, and A.E. Stuchbery, Z. Phys. A **336**, 239 (1990).

[49] R. Ma, Y. Liang, E.S. Paul, N. Xu, D.B. Fossan, L. Hildingsson, and R.A. Wyss, Phys. Rev. C **41**, 717 (1990).

[50] E.S. Paul et al., Phys. Rev. C **58**, 801 (1998).

[51] R. Aryaeinejad, D.J.G. Love, A.H. Nelson, P.J. Nolan, P.J. Smith, D.M. Todd, and P.J. Twin, J. Phys. G **10**, 955 (1984).

[52] M. Palacz, Z. Sujkowski, J. Nyberg, J. Bacelar, J. Jongman, W. Urban, W. Hesselink, J. Nasser, A. Plompen, and R. Wyss, Z. Phys. A **338**, 467 (1991).

[53] K. Hauschild et al., Phys. Rev. C **54**, 613 (1996).

[54] F. Brandolini et al., Phys. Rev. C **60**, 024310 (1999).

[55] W.F. Piel, Jr., C.W. Beausang, D.B. Fossan, L. Hildingsson, and E.S. Paul, Phys. Rev. C **35**, 959 (1987).

[56] P.H. Regan et al., Nucl. Phys. **A533**, 476 (1991).

[57] E.S. Paul, R. Ma, C.W. Beausang, D.B. Fossan, W.F. Piel, Jr., S. Shi, N. Xu, and J.-y. Zhang, Phys. Rev. Lett. **61**, 42 (1988).

[58] D.J. Hartley et al., Phys. Rev. C **63**, 041301(R) (2001).

[59] Y.S. Chen, S. Frauendorf, and L.L. Riedinger, Phys. Lett. B **171**, 7 (1986).

[60] N. Tajima, Nucl. Phys. **A572**, 365 (1994).